





## Research Article

# Simulation Study on the Impact Response of Barrels with Different Rifling Profiles during Bullet Engraving

Zhifang Wei <sup>1</sup>, Yangyang Cheng <sup>2</sup>, Zhiwei Wang <sup>3</sup>, and Yanpeng Lin <sup>4</sup>

<sup>1</sup>College of Mechatronics Engineering, North University of China, No. 3, Xueyuan Road, Taiyuan, Shanxi, China

<sup>2</sup>School of Control Science and Engineering, Shandong University, Jingshi Road, 250061 Jinan, China

<sup>3</sup>No. 208 Institute of China Ordnance Industry, Beijing 102202, China

<sup>4</sup>Chongqing Changan Industry (Group) Co. Ltd., No. 599, Konggang Road, Yubeiqu, Chongqing, China

Correspondence should be addressed to Zhifang Wei; [wzhifang@nuc.edu.cn](mailto:wzhifang@nuc.edu.cn)

Received 18 November 2021; Accepted 21 January 2022; Published 21 February 2022

Academic Editor: Dimitrios E. Manolakos

Copyright © 2022 Zhifang Wei et al. This is an open access article distributed under the Creative Commons Attribution License, which permits unrestricted use, distribution, and reproduction in any medium, provided the original work is properly cited.

Gun barrel bores are prone to ablative damage and stress concentration under high temperatures, pressures, and dynamic load impacts during bullet engraving, which may result in barrel failure. A dynamic stress analysis during bullet engraving is a prerequisite for barrel life analysis and design. Impact responses during bullet engraving were investigated in this study for rifled barrels with different cross-sectional profiles to improve the match between the dynamic performances of the gun barrel and bullet and effectively extend the barrel service life. First, feature suppression by expression based on a uniform parametrized template was used to perform parametric modeling of a gun barrel with rectangular, trapezoidal, multiarc, and multilateral-arc rifling profiles. Second, theoretical models were constructed considering different rifling structures: a model to calculate the chamber pressure, a model for heat transfer in the barrel during continuous firing, and a model to calculate the friction between a bullet and the barrel wall surface based on shear-slip friction theory. These models were integrated into a simulation, where the ABAQUS (ABAQUS. 6.14.1-4. 2014. DASSAULT SIMULIA.)/Explicit software was used to build a finite element model of the barrel dynamic stress under heat-force-friction coupling during bullet engraving. Finally, the dynamic response stresses were analyzed for bullet engraving into four barrels with different rifling profiles. All four types of barrels developed considerable stress at the junction between the forcing cone and the rifled bore under the same impact load. The stress values of the multiarc and multilateral-arc rifling were far below that for the rectangular and trapezoidal rifling. Thus, the barrels with multiarc and multilateral-arc rifling profiles had a higher impact resistance than the other two barrel types.

## 1. Introduction

The barrel is an important structural component of firearms, and the strength of the barrel bore affects important tactical indicators, such as the barrel life, shooting accuracy, and muzzle velocity. A barrel bore consists of a cartridge chamber, forcing cone, and rifled bore. The rifled bore may have different cross-sectional profiles, i.e., rectangular, trapezoidal, multiarc, and multilateral-arc. During bullet engraving, the barrel bore is affected by the pressure of gunpowder combustion gases, the force exerted by bullet insertion, the guide-side resistance, high temperatures, and other factors, which tend to cause ablative damage and crack propagation in the barrel rifling and thus barrel failure [1]. The engraving

of a bullet into a barrel is an important research area for designing bullets to match rifled barrels. It is extremely important to consider the forcing cone and rifled bore for improving the design and extending the service life of a barrel.

An analysis of the barrel impact response during bullet engraving is a prerequisite for barrel life analysis and design and has been extensively studied by domestic and foreign scholars. Ding et al. and Shen et al. both proposed novel finite element mesh generation methods for worn gun barrels to analyze the bullet-barrel interaction [2, 3]. Ekansh [4] used the ANSYS software to simulate the transient response of a T-finned machine gun barrel during bullet engraving. Fan and He [5] addressed large deformation

contact problems caused by friction from interference fit during bullet engraving by building a finite element analysis model for projectiles engraving into a barrel. The engraving of lead-core projectiles was numerically simulated to analyze the deformation behavior of bullet jackets and lead cores before and after engraving. Wu et al. [6, 7] developed an engraving simulation device to experimentally study the quasistatic and dynamic processes of a rotating band engraving into a barrel, and the deformation speed and temperature were found to significantly affect the deformation behavior of the rotating band during real engraving. Zou et al. [8] proposed a novel model for the friction between a rotating band and a gun barrel based on the deformation mechanism of the rotating band during projectile engraving. List et al. [9] derived an accurate formula for the friction coefficient of a barrel-projectile friction pair by developing a hydrodynamic lubrication friction model and comprehensively considering the extreme working conditions of the high pressure and speed of the friction pair. Shen et al. [3] performed a numerical calculation of projectile motion in a barrel assuming a constant projectile-barrel friction coefficient. Ding et al. [2] studied the influence of a worn barrel on interior ballistics and developed a friction model with a temperature-dependent friction coefficient. Lan [10] used a finite element numerical simulation to analyze the effect of the temperature field on the bullet-barrel interaction and firing accuracy. Lu et al. [11] studied the effect of the throat angle on the force on the forcing cone during engraving. Three-dimensional finite element models were constructed for different throat angles, considering the structural properties of the barrel and bullet and constitutive nonlinearity. The model was used to determine the change in the engraving resistance with the engraving displacement at different throat angles. Gao et al. [12] used the Ansys Workbench software to simulate the effects of different throat angles and friction coefficients on the resistance during projectile engraving.

The aforementioned studies focus on methods for analyzing the dynamic stress during projectile engraving into a barrel. The impact of bullet-barrel friction or the temperature field on the response of the projectile engraving to the barrel is investigated in some studies, whereas the impact of the throat angle on the response of the projectile engraving to the barrel is considered in other studies. Note that most of these studies were based on rectangular rifling profiles and did not comprehensively consider the effect of heat-force-friction coupling for the bullet/barrel interaction process. Remington Arms (USA) employs multiarc or multilateral-arc rifling to ensure barrel life and firing accuracy. Therefore, research on how different rifling structures affect the response of a projectile engraving to a barrel is very significant for improving the structural design and fatigue life of a gun barrel. Hence, the impact response of rifled barrels with different cross-sectional profiles during projectile engraving was investigated in this study.

Based on the work of “analysis of impact characteristics and fatigue life of multistrand recoil spring for guns” [13], a uniform parametrized barrel template was constructed based on feature suppression by expression using the UG

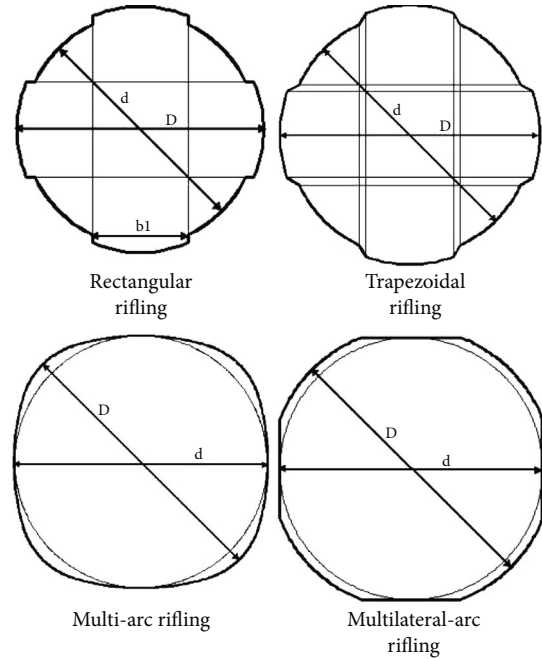


FIGURE 1: Cross-sectional profiles of rifled barrels.

NX (Unigraphics NX, 8.0, 2011, Siemens) software, and efficient three-dimensional models were created for different barrel structures with rectangular, trapezoidal, multiarc, and multilateral-arc rifling. Theoretical analysis models for the chamber pressure during projectile engraving into a barrel, barrel temperature distribution during continuous firing, and friction between bullet and barrel were reviewed and used to construct theoretical models considering different rifling structures: a chamber pressure calculation model, a barrel heat transfer model, and a model for calculating the friction between a bullet and the wall surface of a barrel bore. Thus, the heat-force-friction coupling effect was comprehensively considered, and the ABAQUS/Explicit software was used to build a finite element analysis model for the dynamic response stress during the engraving of a bullet into a barrel. Finally, the effect of the rifling profile on the impact response during projectile engraving was determined by analyzing the dynamic response stress during bullet engraving for four barrels with different rifling profiles.

## 2. Parametric Modeling for Barrels with Different Rifling Profiles Based on Feature Suppression by Expression

Small-caliber rifle barrels were considered in this study. Geometric models were constructed for barrels with rectangular, trapezoidal, multiarc, and multilateral-arc rifling, all of which adopted 4 rifling, and the cross-sectional profiles are shown in Figure 1. The fit between the rifling bone and the bullet was mainly based on the ratio of the cross-sectional area of the cylindrical portion of the bullet  $S_2$  to the inner cross-sectional area of the rifled section  $S$ . In order to

make the barrel sealed during bullet engraving,  $S_z$  must be larger than  $S$ , where the  $S_z/S$  ratio is generally set between 1.01 and 1.03. A large  $S_z/S$  is needed for rectangular and trapezoidal rifling to ensure barrel sealed because of sharp corners at the land/groove junctions, whereas a small  $S_z/S$  can be used

$$S \approx \begin{cases} \frac{\pi d^2}{4} + nb_1 h, & \text{Rectangular rifling,} \\ \frac{\pi d^2}{4} + nb_1 h, & \text{Trapezoidal rifling,} \\ n \left[ \frac{\pi}{180^\circ} \alpha R^2 + \frac{\pi}{180^\circ} \beta r^2 - \left( R - \frac{d}{2} \right) \left( \frac{D}{2} - r \right) \sin \frac{180^\circ}{n} \right], & \text{Multi-rac rifling,} \\ \pi r^2 + \pi \left( \frac{d^2}{5} - r^2 \right) t g \frac{180^\circ}{n}, & \text{Multilateral-arc rifling.} \end{cases} \quad (1)$$

Different features, such as the rifled section, cartridge chamber, muzzle, and contour, were included in each three-dimensional barrel model. A variety of structural types were considered for each feature. For example, rectangular, trapezoidal, circular, and multiarc profiles were considered for the rifled section. Hence, over a thousand parametrized templates were available for parametric modeling of various barrels. Traditional parametric modeling methods involve high computational costs and the storage and management of numerous templates. In this study, a parametrized template was developed based on feature suppression by expression using UG NX software. Multiple types of structures were integrated into a single model to simplify the modeling and management of numerous templates. The category and structural characteristics of each barrel feature were analyzed, and a physical model was developed for a specific structural type for each feature. The function relationship and constraint relationship among the model dimension parameters were analyzed. The UG NX expression was used to define the key dimension parameters of a barrel (e.g., the barrel length, groove size, and outer barrel diameter), and related functional relations were established. Table 1 presents the drive parameters, including the muzzle shape, number of cones in the cartridge chamber, number of grooves, rifling profile, and contour parameters. The drive expression was used in feature suppression to formulate a uniform parametrized barrel template incorporating the constraint relation. That is, the barrel substrate model was used to create physical models of features with various structures (the rifling bone, cartridge chamber, muzzle, and contour). For instance, physical models were developed for the rifled section with rectangular, trapezoidal, multiarc, and multilateral-arc cross-sections, as shown in Figure 2. Finally, the values of the respective dimensional expressions were modified based on design requirements to generate three-dimensional models of barrels with different structural types and dimensions using the parametrized template. The uniform parametrized template was thus used to realize parametric modeling of barrels with over a thousand structural types.

for multiarc and multilateral-arc rifling for which there is a smooth transition between the adjacent groove and land. The cross-sectional areas of rifled sections of specific profiles are given in Equation (1).

### 3. Theoretical Models

*3.1. Model for Calculating the Chamber Pressure of Barrels with Different Rifling Profiles.* The large quantity of gas generated during gunpowder combustion pushes a bullet out of a barrel chamber via an extremely complex process. The change in the chamber pressure and bullet velocity with the displacement and time can be determined by analyzing the rule for gunpowder combustion, the rule for energy conversion during firing, and the pattern of bullet motion and establishing a system of equations to reflect these constraints. The cross-sectional profile of a rifled barrel can also affect this process. The variation pattern of the chamber pressure during firing in barrels with different rifling profiles can be determined by building interior ballistic calculation models for these barrels, as shown in

$$\begin{cases} \psi = \begin{cases} \chi Z(1 + \lambda Z + \mu Z^2), \\ \chi_s \frac{Z}{Z_k} \left( 1 + \lambda_s \frac{Z}{Z_k} \right), \\ 1, \end{cases} \\ \frac{dZ}{dt} = \frac{u_1 p^n}{e_1}, \\ \varphi m \frac{dv}{dt} = Sp, \\ Sp(l_\psi + l) = f\omega\psi - \frac{\theta}{2}\varphi m v^2, \\ l_\psi = l_0 \left[ 1 - \frac{\Delta}{\rho} (1 - \psi) - \alpha \Delta \psi \right]. \end{cases} \quad (2)$$

In the equation presented above,  $\psi$  is the percentage of burnt gunpowder;  $\chi$ ,  $\lambda$ ,  $\chi_s$ , and  $\lambda_s$  are shape characteristic parameters for gunpowder;  $Z_k$  is the relative value of the burnt thickness of the gunpowder grains after combustion;

TABLE 1: Drive parameters for the parametrized barrel template.

Rifling bone design parameters	Rifling shape
	Rifling number
	Land diameter
	Groove depth
	Rifling width
	Lead
	Groove direction
Cartridge chamber design parameters	Number of cones
	The distance from the first cone to the end of the barrel
	The distance from the second cone to the end of the barrel
	Diameter of large end of the first cone
	Diameter of large end of the second cone
Muzzle design parameters	Diameter of small end of the second cone
	Cartridge chamber grooving
	Muzzle shape
	External fillet of muzzle
Contour parameters	Fillet inside the muzzle
	Outer diameter of muzzle
	Outer diameter at the maximum chamber pressure
	Barrel length

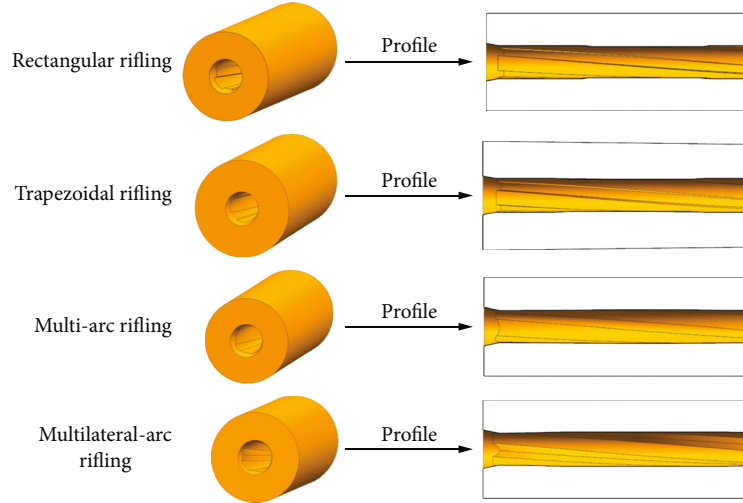


FIGURE 2: Parametrized template for barrels with different rifling section structures.

$\omega$  is the gunpowder charge;  $u_1$  is the gunpowder burning rate coefficient;  $n$  is the pressure index;  $p$  is the gunpowder combustion gas pressure;  $e_1$  is one-half of the initial thickness of the gunpowder grain;  $m$  is the bullet mass;  $\varphi$  is the coefficient of secondary work, neglecting the work done by the engraving resistance;  $S$  is the cross-sectional area of the rifled section (which varies with the rifling profile);  $l$  is the bullet travel;  $l_\psi$  is the ratio of the free volume of the chamber to the cross-sectional area of the rifled section;  $f$  is the gunpowder force capacity;  $v$  is the bullet velocity;  $\theta = k - 1$ , where  $k$  is the adiabatic coefficient;  $l_0$  is the ratio of the chamber volume to the cross-sectional area of the rifled section;

$\Delta$  is the gunpowder loading density;  $\rho$  is the gunpowder density; and  $\alpha$  is the gunpowder covolume.

**3.2. Barrel Heat Transfer Model.** During firing, heat is transferred between the gunpowder combustion gas and barrel and between the barrel and ambient air through conduction, convection, and radiation. Heat is transferred from the inner to outer wall of the barrel through conduction and from the inner and outer walls of the barrel to the surrounding media through convection and radiation. Radiative heat transfer is less than 1% of convective heat transfer and was therefore neglected in this study. A mathematical transient heat

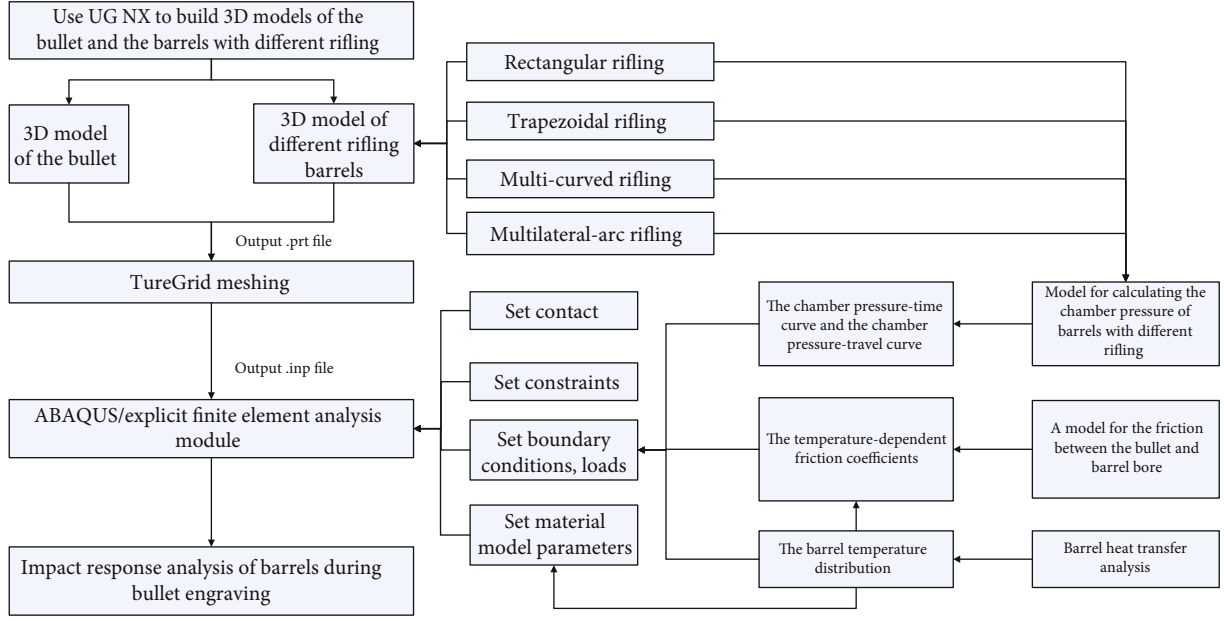


FIGURE 3: Cosimulation process for the barrel impact response.

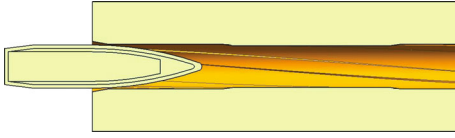


FIGURE 4: Three-dimensional models of barrels and bullets.

transfer model was built based on heat conduction and heat convection theories and is shown in

$$\rho c(T) \frac{\partial T}{\partial t} = \frac{\partial}{\partial x} \left( k_x(T) \frac{\partial T}{\partial x} \right) + \frac{\partial}{\partial y} \left( k_y(T) \frac{\partial T}{\partial y} \right) + \frac{\partial}{\partial z} \left( k_z(T) \frac{\partial T}{\partial z} \right) + Q. \quad (3)$$

In the equation presented above,  $\rho$  and  $c(T)$  are the density and specific heat capacity of the barrel material, respectively;  $T$  represents the barrel material temperature;  $k_x$ ,  $k_y$ , and  $k_z$  are the thermal conductivities in the three coordinate directions, respectively; and  $Q$  denotes the internal heat source, which is normally referred to as heat converted from plastic work.

**3.3. Model for the Friction between a Bullet and the Inner Barrel Wall.** During the engraving of a bullet into the rifling, the cylindrical portion of the bullet intersects with the rifling, and the bullet jacket surface is subjected to plastic deformation and friction with grooves and lands. Shear-slip friction theory was used to formulate a model for the friction between the bullet and barrel bore, as shown in

$$f = \begin{cases} \mu_d \sigma_n, & \mu_d \sigma_n \leq \tau_s, \\ \tau_s, & \mu_d \sigma_n > \tau_s, \end{cases} \quad (4)$$

where  $f$  represents the shear stress caused by friction on the contact interface;  $\sigma_n$  denotes the normal positive stress of contact between the bullet and the inner barrel wall;  $\tau_s$  denotes the maximum shear stress of the material; and  $\mu_d$  is the dynamic friction coefficient between the bullet and the inner barrel wall and depends on the temperature of the inner barrel wall, as given by Equation (5) [14].

$$\mu(T) = 2 \times 10^{-11} T^4 - 2.963 \times 10^{-8} T^3 + 1.323 \times 10^{-5} T^2 - 0.002T + 0.384. \quad (5)$$

The shear stress between the bullet and the inner barrel wall also depends on the temperature of the inner barrel wall, as shown in

$$\tau_{\max} = \left\{ a_1 \exp \left[ - \left( \frac{T - 500}{b_1} \right)^2 \right] \right\}, \quad (6)$$

where  $a_1$  and  $b_1$  are design parameters.

Combining Equations (4), (5), and (6) based on the Zorev friction model yields the following equation.

$$\begin{cases} \mu(T) = 2 \times 10^{-11} T^4 - 2.963 \times 10^{-8} T^3 + 1.323 \times 10^{-5} T^2 - 0.002T + 0.384, \\ \tau_{\max} = a_1 \exp \left[ - \left( \frac{T - 500}{b_1} \right)^2 \right], \\ \tau = \min(\mu \sigma_n, \tau_{\max}). \end{cases} \quad (7)$$

## 4. Finite Element Analysis Model for the Barrel Impact Response under Heat-Force-Friction Coupling

### 4.1. Basic Hypotheses

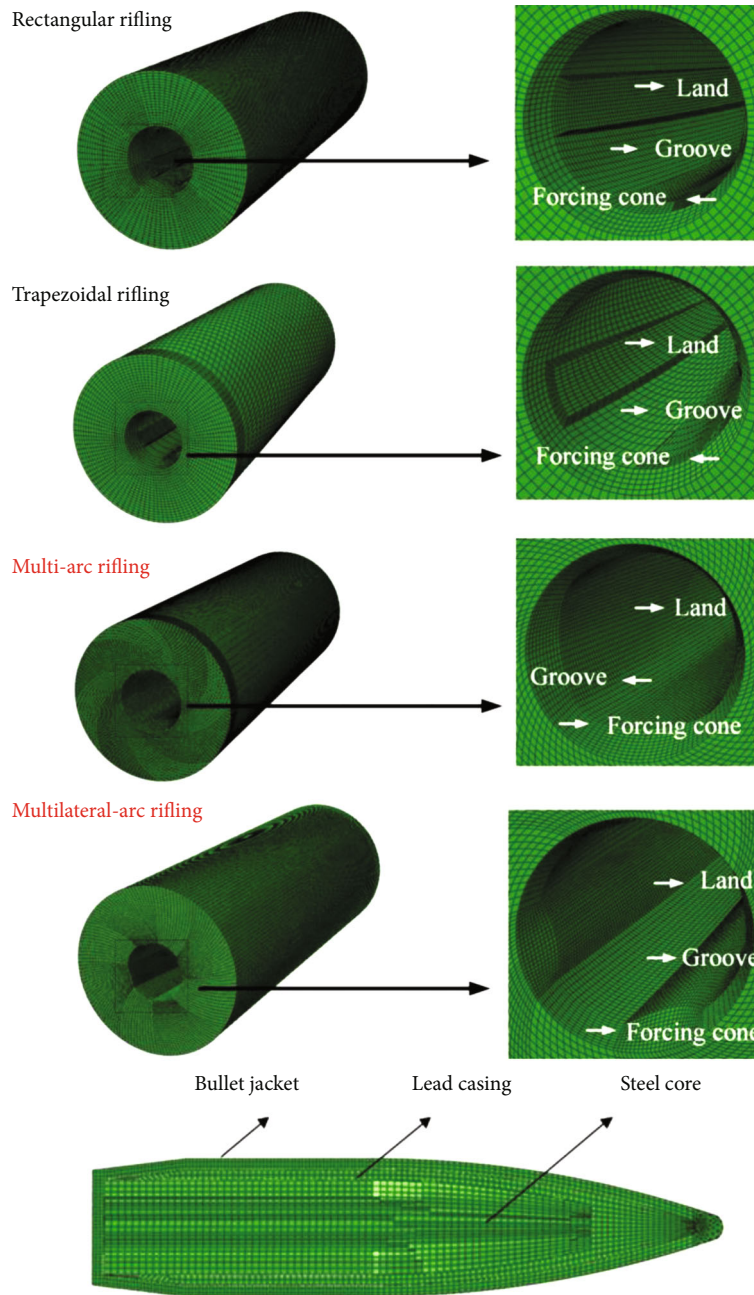


FIGURE 5: Mesh models of barrels with different rifling profiles and bullets.

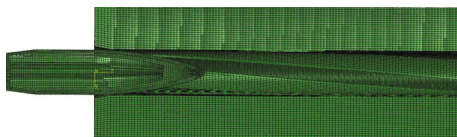


FIGURE 6: Mesh models of partial barrels and bullets.

(1) Idealized models of the barrel and bullet are formulated that do not consider the effect of structures such as the barrel gas port and the tight mouth grooves on the bullet tail

- (2) The effect of the air resistance at the front of the projectile on projectile motion is neglected, and the projectile base pressure is replaced with the mean pressure
- (3) The materials of the barrel and bullet are assumed to be homogeneous and isotropic

4.2. *Cosimulation Process of the Barrel Impact Response to Bullet Engraving under Heat-Force-Friction Coupling.* The engraving of a projectile into the barrel rifling under gunpowder combustion gas pressure involves heat-force-friction coupling. The barrel impact response to engraving can directly affect damage to and the fatigue life of the barrel.

TABLE 2: Parameters of the barrel substrate material.

Temperature (K)	Density (kg/mm <sup>3</sup> )	Young's modulus (MPa)	Poisson's ratio	Thermal conductivity (W/(m.K))	Specific heat (J/(kg.K))	Coefficient of thermal expansion (K <sup>-1</sup> )
298.15	7.85e-6	2.08e+05	0.26	45.2	539.8	1.3e-5
498.15	7.85e-6	1.81e+05	0.27	38.1	576.1	1.3e-5
698.15	7.85e-6	1.66e+05	0.29	34.1	607.5	1.3e-5
848.15	7.85e-6	1.55e+05	0.31	31.3	634.7	1.3e-5
1098.15	7.85e-6	1.47e+05	0.34	29.3	658.2	1.3e-5
1298.15	7.85e-6	1.41e+05	0.36	27.7	678.5	1.3e-5

TABLE 3: Basic data for the bullet jacket material.

Temperature (K)	Density (kg/mm <sup>3</sup> )	Young's modulus (MPa)	Poisson's ratio	Thermal conductivity (W/(m.K))	Specific heat (J/(kg.K))	Coefficient of thermal expansion (1/K)
298.15	8.9e-9	1.24e+05	0.33	390.1	383.3	2.1e-5
399.15	8.9e-9	1.17e+05	0.33	381.7	400.2	2.1e-5
522.15	8.9e-9	1.07e+05	0.33	363.2	412.4	2.1e-5
654.15	8.9e-9	1.00e+05	0.33	349.6	425.8	2.1e-5
771.15	8.9e-9	0.95e+05	0.33	343.8	437.5	2.1e-5
900.15	8.9e-9	0.90e+05	0.33	337.8	450.3	2.1e-5

TABLE 4: Basic data for lead and steel.

Material	Density/t × mm <sup>3</sup>	Poisson's ratio	Young's modulus/MPa
Lead	1.13e-08	0.42	17000
Steel	7.86e-09	0.3	207000

TABLE 5: Parameters of the Johnson-Cook model for the bullet jacket material.

A/MPa	B/MPa	C	n	M	T <sub>melt</sub> /K	T <sub>room</sub> /K
90	292	0.01	0.42	0.68	1189	293

TABLE 6: Parameters of the Johnson-Cook damage model for the bullet jacket material.

D <sub>1</sub>	D <sub>2</sub>	D <sub>3</sub>	D <sub>4</sub>	D <sub>5</sub>
0.54	4.89	-3.03	0.014	1.12

TABLE 7: Parameters of the Johnson-Cook model for the lead casing material.

A/MPa	B/MPa	C	n	M	T <sub>melt</sub> /K	T <sub>room</sub> /K
14	17.6	0.685	0.035	1.68	600	293

To study the effect of different types of cross-sectional profiles of rifled barrels on projectile engraving, finite element analysis models were developed for the impact response of

barrels with rectangular, trapezoidal, multiarc, and multilateral-arc rifling to bullet engraving. The cosimulation process of the barrel impact response under heat-force-friction coupling to projectile engraving is shown in Figure 3. The Runge-Kutta method was used to solve the interior ballistic equations presented above, and the chamber pressure-time curve and the chamber pressure-travel curve were plotted for barrels with different rifling profiles. A VUAMP subprogram was developed to calculate the chamber pressure load and imported into ABAQUS finite element simulation software. The thermal impact of the gunpowder combustion gas produces changes in the material properties of the barrel and projectile and introduces a temperature dependence into the mechanical response of the rifling to projectile engraving. A heat transfer analysis was performed to determine the barrel distribution temperature, and a model for the projectile engraving into the barrel was built for the corresponding temperature state. A VFRIC friction subprogram was written in Fortran based on the friction model with variable friction coefficients. The ABAQUS solver was used to embed the temperature-dependent friction model into a simulation of bullet engraving, and the VFRIC friction subprogram was called to incorporate the temperature-dependent friction coefficients.

**4.3. Geometric Modeling and Meshing.** Barrels of small-caliber rifles and matching normal bullets were considered in this study. The aforementioned parametric modeling methods were used to construct three-dimensional geometric models of barrels with rectangular, trapezoidal, multiarc, and multilateral-arc rifling. Three-dimensional solid models were constructed for a bullet [15] and a barrel 50 mm from the entrance of the forcing cone to study the impact

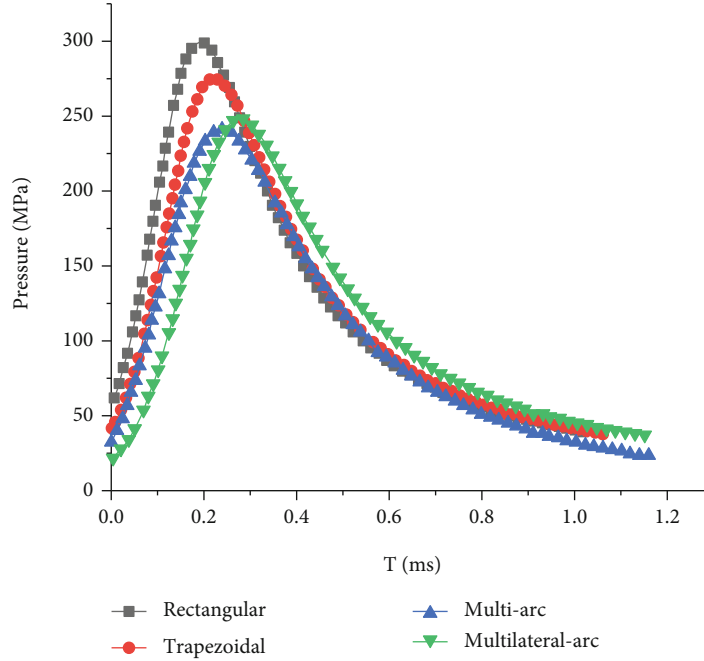


FIGURE 7: Chamber pressure-time curves.

TABLE 8: Maximum chamber pressures corresponding to different cross-sectional profiles.

Rifling section shape	The maximum chamber pressure/MPa	Deviation/MPa	Percentage/%
Rectangular	299.6	0	0
Trapezoidal	274.8	-24.8	-8.2
Multiarc	248.7	-50.9	-17
Multilateral-arc	249.5	-50.1	-16.7

response process from the beginning to the completion of bullet engraving into the forcing cone with high computational efficiency. Assembly drawings of barrels and bullets are shown in Figure 4. TrueGrid software was used to perform hexahedral meshing for barrels with different rifling profiles and projectiles, and mesh refinement was implemented for important areas, such as the forcing cone and lands. The unit type was set to C3D8RT. Figure 5 shows the finite element mesh models of barrels with different rifling profiles and bullets. Mesh models of selected barrels and bullets are shown in Figure 6. The mesh data file \*.inp was imported into ABAQUS, and the ABAQUS/Explicit module was used to build a finite element model for the explicit dynamic analysis of the projectile engraving process.

**4.4. Material Models.** The barrel substrate material was 30SiMnMoVA. An isotropic plastic model conforming to the Huber-Mises yield criterion was defined for the material, where the model parameters are shown in Table 2.

Normal bullets typically have three components, i.e., a bullet jacket, lead casing, and steel core. The bullet jacket

was made of H90, for which the basic parameters are shown in Table 3. Basic data for lead and steel are shown in Table 4.

The bullet jacket surface is scored by rifling, and the material yields during the engraving of the bullet into the forcing cone via a complex nonlinear process with a high strain rate. A Johnson-Cook model was defined for the bullet jacket material and is given by

$$\begin{cases} \sigma = (A + B\epsilon^n)(1 + C \ln \dot{\epsilon}^*)(1 - T^{*m}), \\ T^* = \frac{T - T_{\text{melt}}}{T_{\text{melt}} - T_{\text{room}}}, \end{cases} \quad (8)$$

where  $\sigma$  is the Von Mises flow stress;  $A$ ,  $B$ ,  $C$ ,  $n$ , and  $m$  are material constants;  $\epsilon$  and  $\dot{\epsilon}^*$  denote the equivalent plastic strain and strain rate, respectively; and  $T$ ,  $T_{\text{melt}}$ , and  $T_{\text{room}}$  denote the test temperature, material melting point, and reference ambient temperature, respectively [16]. The model parameters are shown in Table 5.

Initial damage to a ductile metal proceeds by fracture and necking. The initial damage was modeled using an equivalent plastic strain  $\epsilon_D$ , following the Johnson-Cook initial damage criterion:

$$\dot{\epsilon}_D^{pl} = (D_1 + D_2 \exp(-D_3 \eta)) \cdot \left[ 1 + D_4 \ln \left( \frac{\dot{\epsilon}^{pl}}{\dot{\epsilon}_0} \right) \right] (1 + D_5 \hat{\theta}), \quad (9)$$

where  $D_1$ - $D_5$  are material failure parameters;  $\eta$  denotes the triaxial stress;  $\dot{\epsilon}^{pl}$  denotes the equivalent plastic strain rate;  $\dot{\epsilon}_0$  denotes the equivalent plastic damage strain; and  $\hat{\theta}$  represents



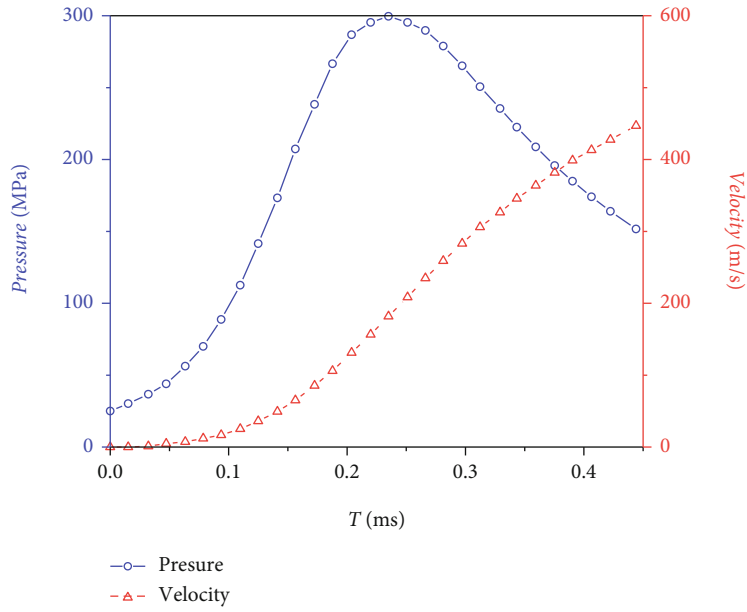


FIGURE 8: Time history curves for the chamber pressure and velocity.

TABLE 9: Calculated and measured maximum chamber pressures.

Parameter	Calculated value	Experimental value	Deviation	Percentage deviation/%
The maximum chamber pressure/MPa	299.6	295.6	4	1.4

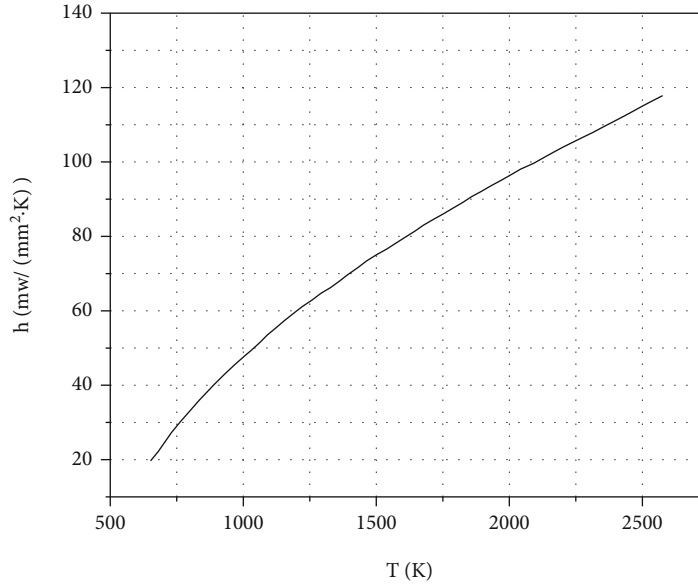


FIGURE 9: Heat convection coefficient of the gunpowder combustion gas.

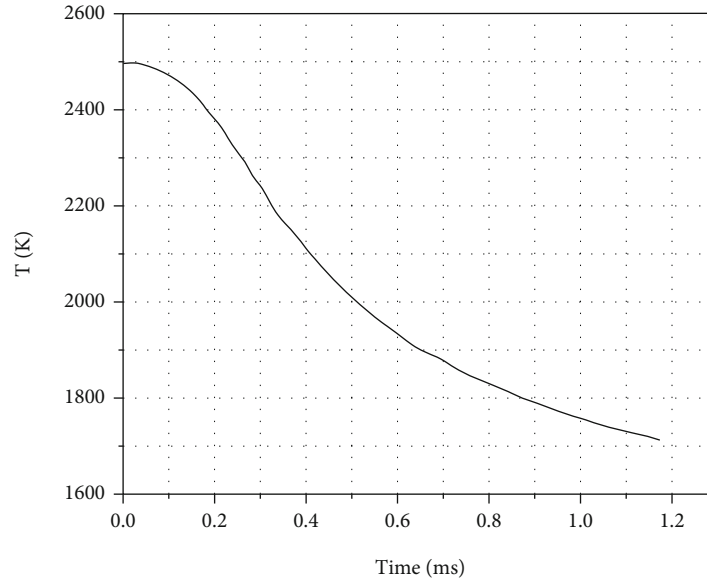


FIGURE 10: Temperature curve of the gunpowder combustion gas.

the dimensionless temperature. The model parameters are shown in Table 6.

A Johnson-Cook model [10] was defined for the lead casing, where the model parameters are shown in Table 7.

#### 4.5. Setting the Load and Boundary Conditions

**4.5.1. Interior Ballistic Calculation for Barrels with Different Rifling Profiles.** In Equation (1), the cross-sectional area  $S$  of the rifled section depends on the rifling profile. A VUAMP program was written to calculate the interior ballistics using the Runge-Kutta method. Figure 7 shows the chamber pressure-time curves of barrels with different rifling profiles obtained by solving Equation (2).

In Figure 7, the barrel with rectangular rifling has a higher maximum chamber pressure than the barrel with trapezoidal rifling, and the maximum chamber pressure of the barrel with multiarc rifling is close to that of the barrel with multilateral-arc rifling but is lower than those of the barrels with rectangular and trapezoidal rifling. The maximum chamber pressures of barrels with different rifling profiles are shown in Table 8.

In Table 8, the maximum chamber pressure for the barrel with rectangular rifling is higher than those of the barrels with trapezoidal, multiarc, and multilateral-arc rifling by 8.2, 17, and 16.7%, respectively.

The calculated interior ballistics results were verified by comparison with the test result for the barrel with rectangular rifling. The calculation was performed over a range beginning from the entrance of the forcing cone to 50 mm along the guide portion. The chamber pressure-velocity curve is shown in Figure 8. The interior ballistic duration is 0.455 ms, and the initial chamber pressure is 25 MPa. The calculated chamber pressure peaks at 299.56 MPa at 0.259 ms, which represents only a 1.4% deviation from the measured maximum chamber pressure, as shown in Table 9.

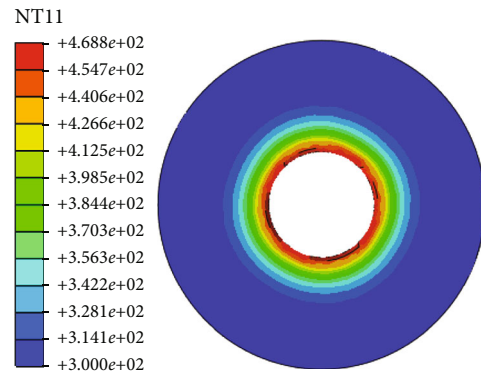


FIGURE 11: Temperature nephogram of the barrel during continuous firing.

**4.5.2. Heat Transfer Analysis of the Barrel.** The barrel heat transfer model was simulated in ABAQUS to determine the radial temperature distribution of the barrel and the temperature distribution at different points of the bore during continuous firing. Heat transfer during firing occurred by convection between the inner barrel wall and the high-temperature gunpowder combustion gas and by heat exchange between the outer barrel wall and the ambient air. Heat exchange between the inner barrel wall and the cold air flowing into the barrel occurred during the air cooling period after the bullet exited the chamber and before the next bullet began to move. The heat convection coefficient between the inner barrel wall and the high-temperature gunpowder combustion gas was determined using Equation (10) and is shown in Figure 9. The heat sink temperature is the temperature of the gunpowder combustion gas and was obtained by solving Equation (11) and Equation (2) for the interior ballistics and is shown in Figure 10. The heat exchange coefficient between the outer barrel wall and the ambient air was set to  $2 \text{ mW}/(\text{mm}^2 \cdot \text{K})$ , and the heat sink temperature was set to room temperature (298.15 K) [17].

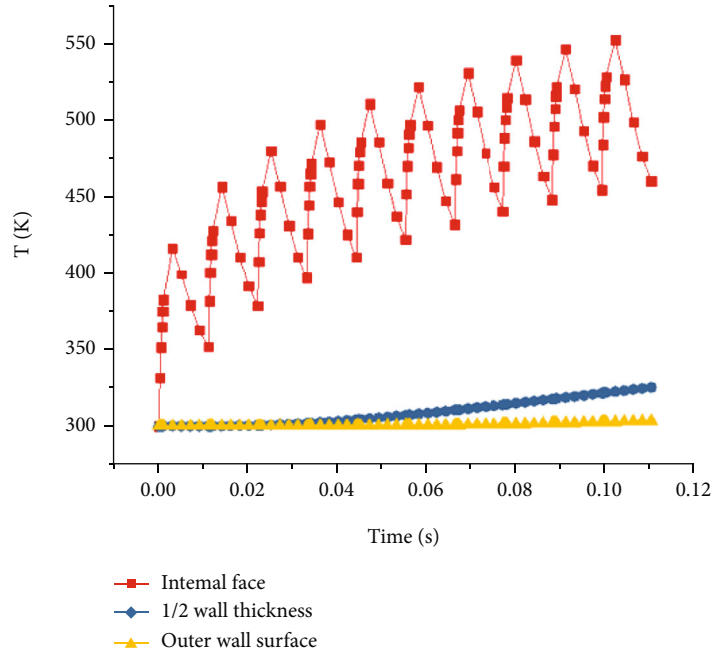


FIGURE 12: Time history curve of the inner wall surface temperature during continuous firing.

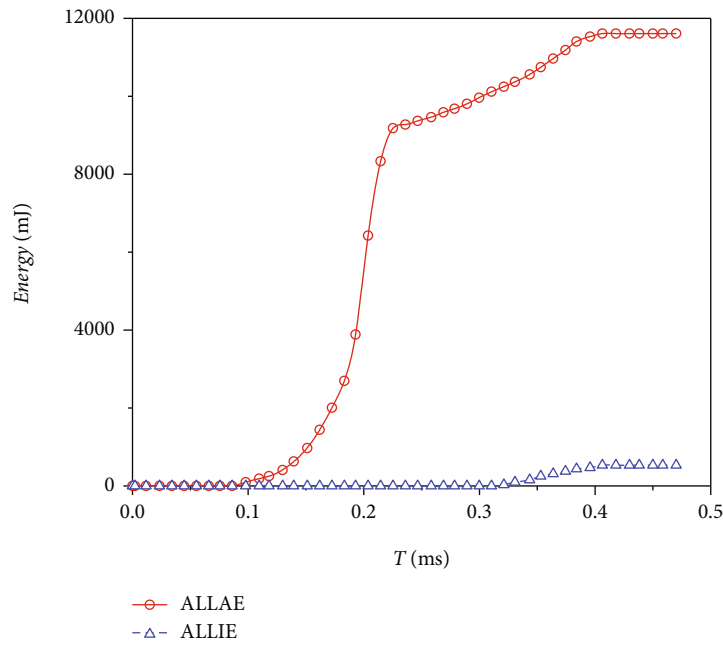


FIGURE 13: Time history curves of the hourglass energy and internal energy.

The heat convection coefficient of the gunpowder combustion gas was calculated as follows:

$$h_c = 0.023 \frac{\lambda}{a} \left[ \frac{v(t)\rho(t)d}{\mu(t)} \right]^{0.8} \left[ \frac{\rho(t)c_p(t)d}{\lambda} \right]^{0.4} K_c, \quad (10)$$

where  $d$  represents the inner barrel diameter;  $\rho(t)$ ,  $v(t)$ ,  $\mu(t)$ ,  $a$ , and  $c_p(t)$  denote the density, velocity, viscosity coefficient, thermal conductivity, and specific heat of the gunpowder

combustion gas, respectively; and  $K_c$  is a correction coefficient ranging from 1.15 to 1.2.

The temperature of the gunpowder combustion gas was calculated as given below.

$$T_g(t) = \left[ 1 - \frac{(k-1)\phi q v(t)^2}{2f\omega\psi} \right] T_b. \quad (11)$$

In this equation,  $k = C_p/C_v$ , where  $C_p$  represents the specific heat capacity of the gunpowder combustion gas at

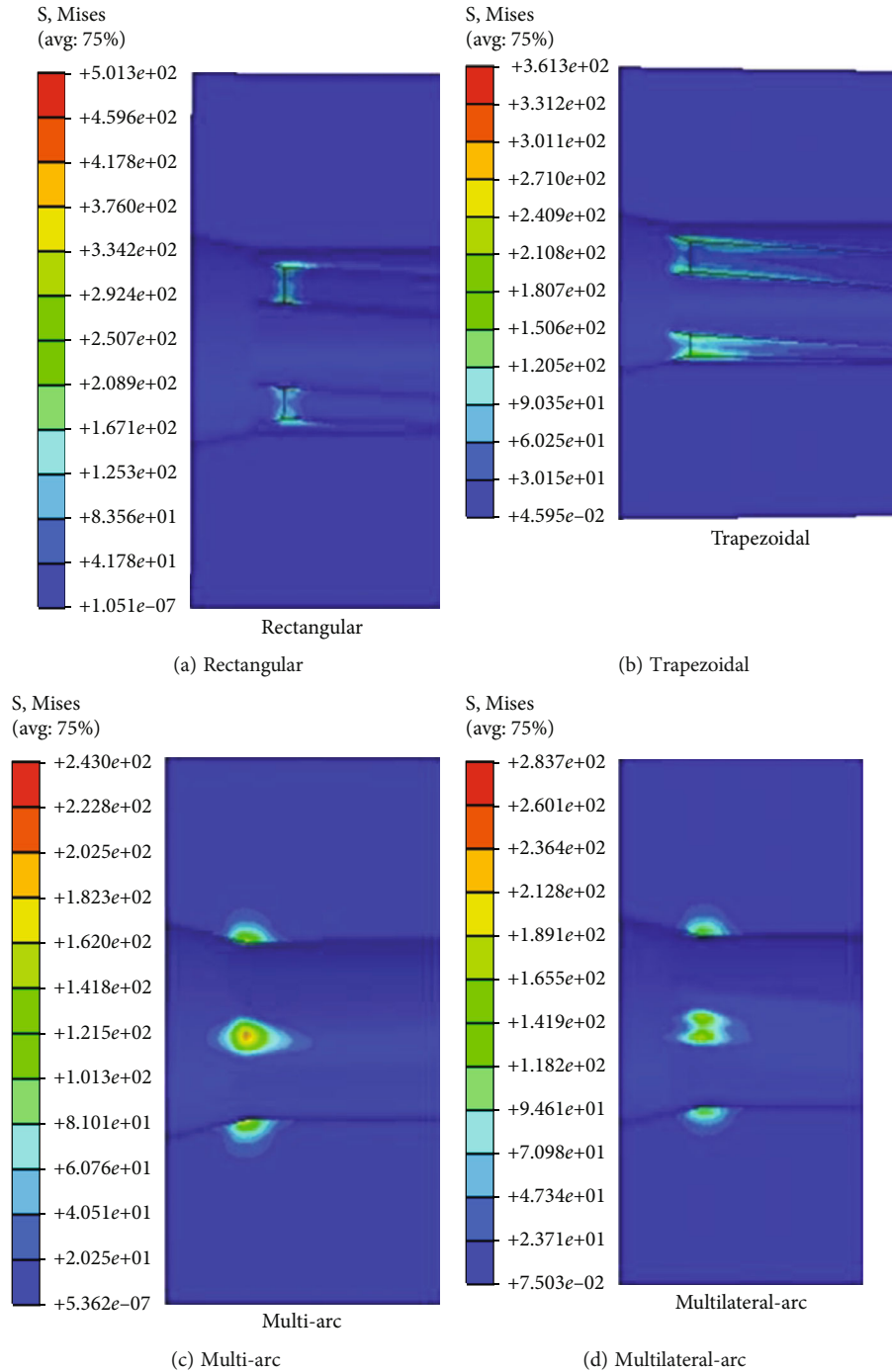


FIGURE 14: Nephograms of the barrel stress at the early stage of bullet engraving into the forcing cone.

constant pressure and  $C_v$  is the specific heat capacity of the gunpowder combustion gas at constant volume;  $f = RT_b$ , where  $R$  and  $T_b$  denote the gas constant and the gunpowder explosion temperature, respectively;  $\varphi$  is a virtual coefficient;  $q$  is the bullet weight;  $v(t)$  is the bullet velocity;  $\omega$  denotes the gunpowder charge; and  $\psi$  is the relative mass of burnt gunpowder.

The radial temperature distribution of the barrel and the variation in the barrel temperature with time during continuous firing are shown in Figures 11 and 12, respectively.

Figure 11 is a temperature nephogram of the barrel section 50 mm away from the entrance of the forcing cone during continuous firing and shows that the temperature gradually decreases from the inner wall to the outer wall. Figure 12 is a time history curve for the barrel temperature during continuous firing, indicating a high peak temperature of the inner barrel wall that increases with the number of shots.

4.5.3. Calculation of the Coefficient of Friction between the Bullet and the Inner Barrel Wall. A VFRIC subprogram

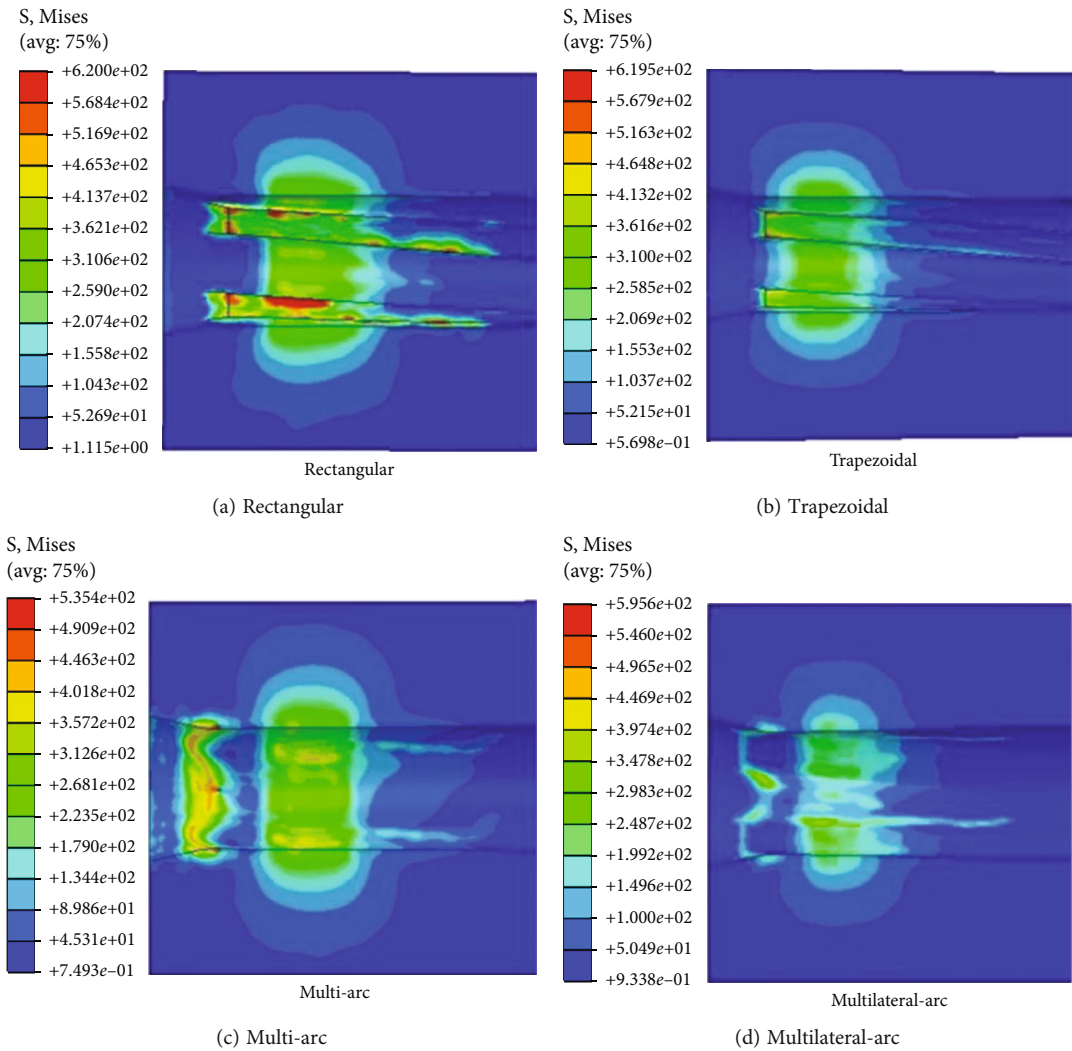


FIGURE 15: Nephograms of the barrel stress at the completion of bullet engraving into the rifled section.

[16] was written in Fortran based on the friction model shown in Equation (7) to calculate the temperature-dependent coefficient of friction between the bullet and the inner barrel wall.

4.5.4. *Setting the Load and Boundary Conditions.* The VUAMP subprogram for calculating the chamber pressure load and the VRIC subprogram for calculating the friction coefficient were imported into ABAQUS as secondary software. The subprograms were loaded using the temperature field determined by the heat transfer analysis of the barrel as the initial temperature field for the barrel impact response analysis during continuous firing [18], based on the cosimulation process presented in Figure 3. Thus, a coupling analysis for heat, force, and friction was realized.

## 5. Simulation Results and Analysis

5.1. *Hourglass Energy.* The hourglass energy should be controlled to below 5% of the total internal energy to ensure accurate and reliable simulation results using reduced inte-

gration elements. Default hourglass control was employed in this study to verify the ratio of the hourglass energy to the total internal energy of the models. Figure 13 shows the time history curves of the ALLAE hourglass energy and ALLIE internal energy. The maximum ALLAE hourglass energy is 534.38 mJ, and the corresponding internal ALLIE energy is 11609.9 mJ. Thus, the ratio of the ALLAE hourglass energy to the ALLIE internal energy is 4.4%, which indicates that the simulation result is reliable.

5.2. *Analysis of Dynamic Stress Response for Barrels with Different Rifling Profiles under Heat-Force-Friction Coupling.* Figures 14, 15, and 16 are nephograms of the Huber-Mises stress for barrels with rectangular, trapezoidal, multiarc, and multilateral-arc rifling during various periods of the bullet engraving into the rifling. Figure 17 shows the time history curves of the stresses at the guide side, middle section, and nonguide side of each land at points at the entrance of the rifled section of the barrels with different rifling profiles. A large stress is induced when the bullet begins to engrave into the forcing cone. As the base pressure

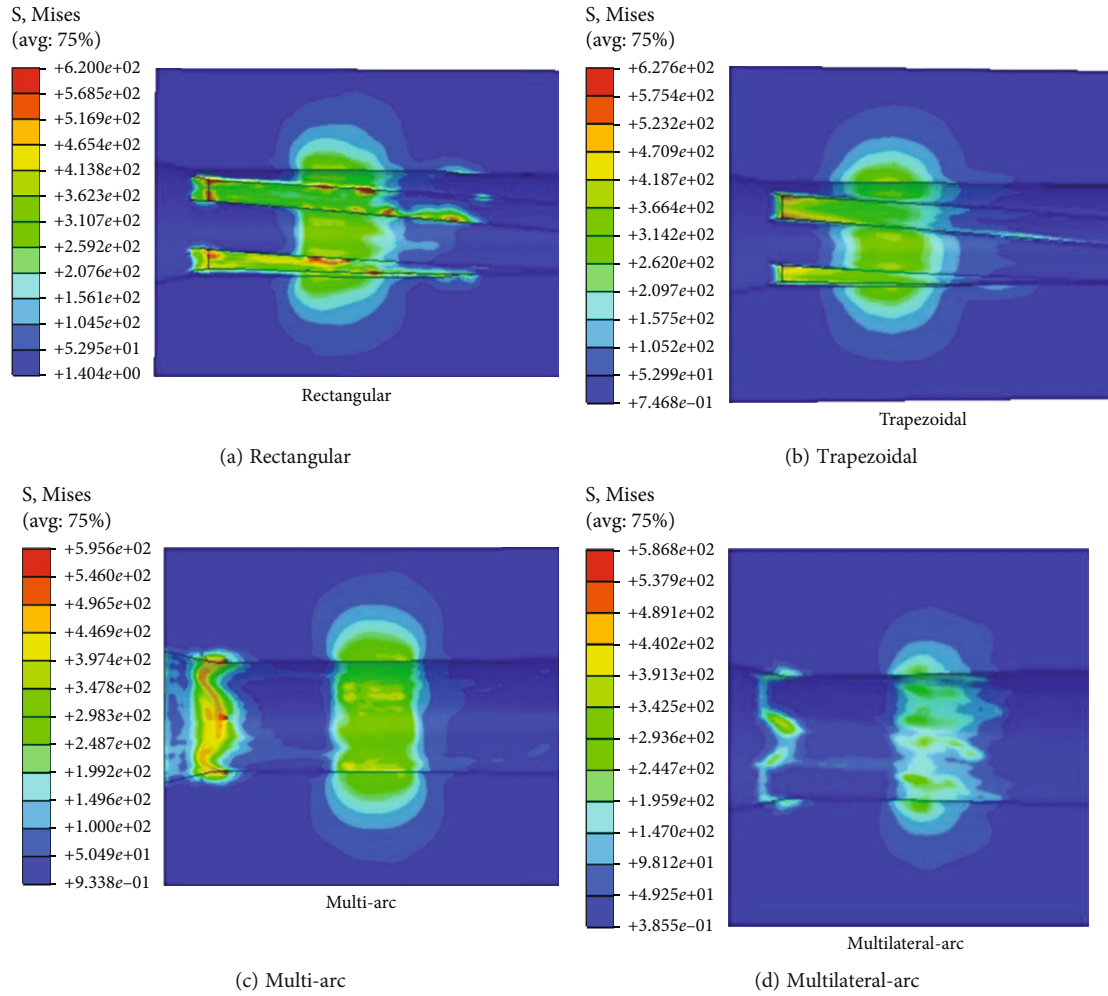
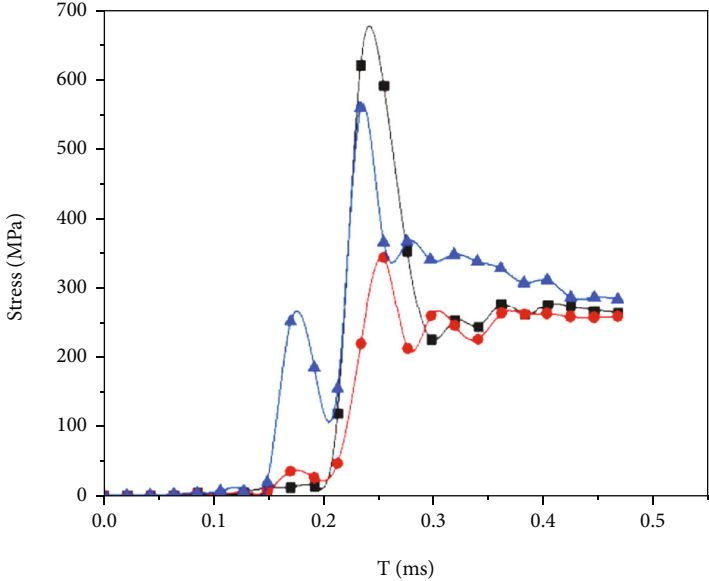


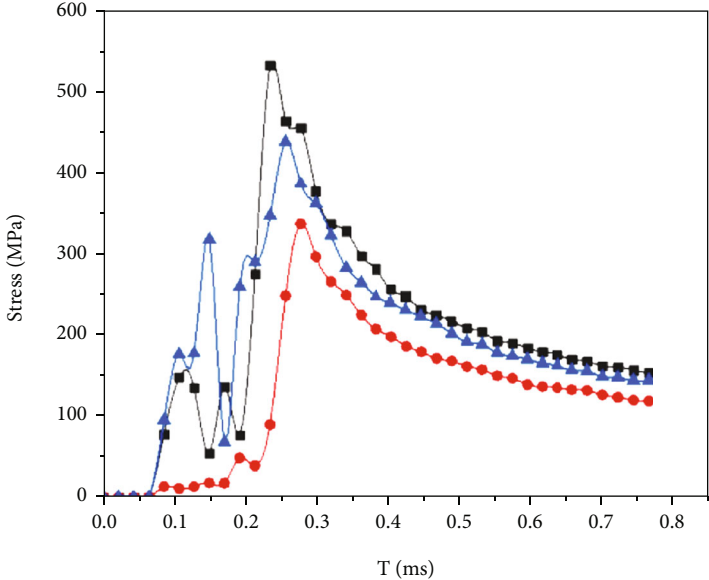
FIGURE 16: Nephograms of the barrel stress under the maximum chamber pressure.

keeps increasing, the bullet continues engraving into the barrel, resulting in a constant increase in the stress at the inner barrel wall. When the entire bullet engraves into the rifled section, the maximum stresses are reached at the land/groove junctions and at the entrance to the rifled section. The stress subsequently trends downward. The stress distribution of the barrel with rectangular rifling is substantially similar to that of the barrel with trapezoidal rifling during bullet engraving, whereas the stresses at the land/groove junctions of the rectangular rifling differ significantly from those of the trapezoidal rifling. The land/groove junctions of the rectangular rifling are prone to stress concentration because the groove interior angle and land exterior angle are approximately right angles. The groove interior angle and land exterior angle of the trapezoidal rifling are not right angles, but stress concentration nevertheless develops at the land/groove junctions. However, the stress concentration is less severe than that developed at the rectangular rifling land/groove junctions. The stress is generally high in lands and considerably higher on both sides than in the middle section, whereas the stress at the guide side is higher than that at the nonguide side. This stress distribution may accelerate land wear during repeated firing, thereby continually

reducing the land size. In addition, the stress distribution for the barrel with multiarc rifling is substantially similar to that in the barrel with multilateral-arc rifling during projectile engraving: there is a high-impact stress at the junction between the forcing cone and the rifled section, a uniform stress distribution over the rifled section, and no discernible stress concentration. The guide-side stress is considerably lower for the barrels with multiarc and multilateral-arc rifling than for the barrels with rectangular and trapezoidal rifling, because the wide lands and large area of the guide side of the barrels with multiarc and multilateral-arc rifling help to reduce the stresses at the top surface and guide side of each land. Therefore, the barrels with multiarc and multilateral-arc rifling profiles have a higher impact resistance than the barrels with the other two types of rifling profiles, which reduces the damage caused by the projectile impact to the bore and effectively increases the barrel service life. A comparative analysis of the results for the four types of barrels shows that the maximum stress develops at the junction between the forcing cone and the rifled bore during projectile engraving. Therefore, severe damage is inflicted near the initial position of the rifled section for all four types of rifled barrels, in accordance with the actual conditions.

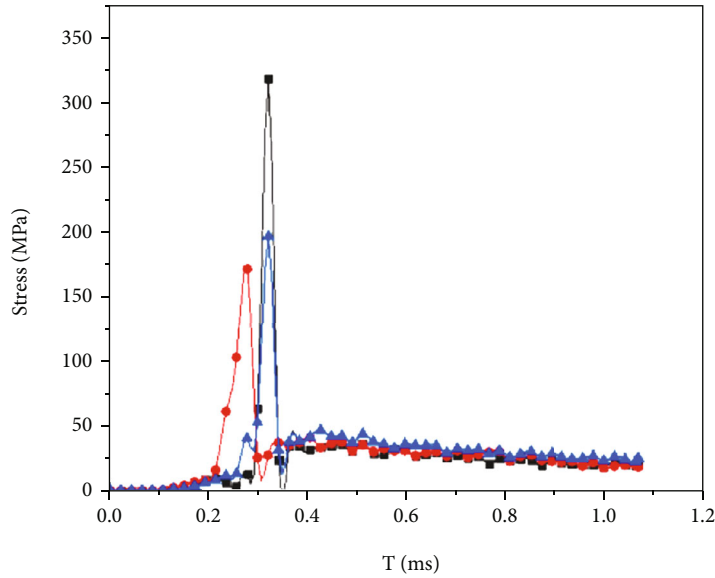


(a) Rectangular

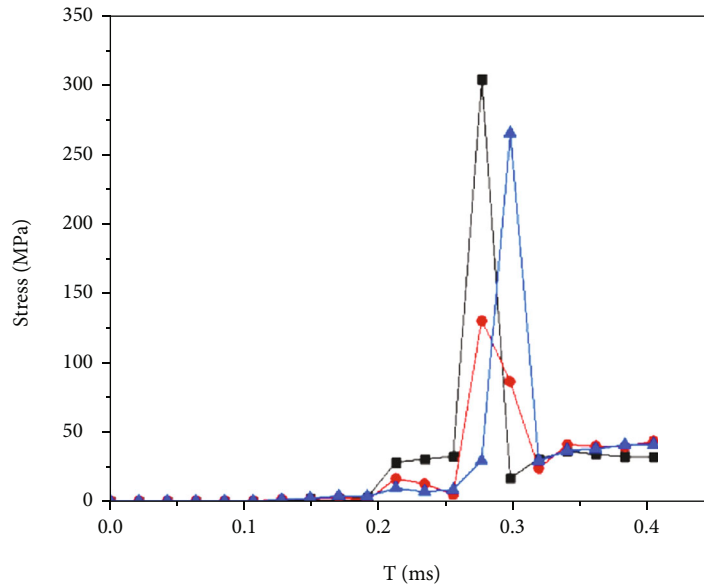


(b) Trapezoidal

FIGURE 17: Continued.



(c) Multiarc



- Guided side
- Middle of land
- ▲ Unguided side

(d) Multilateral-arc

FIGURE 17: Stress distribution in barrels with different cross-sectional profiles.

### 6. Conclusion

Dynamic stress analysis models and methods for barrels with different rifling profiles were applied in this study to bullet engraving into rifling during continuous firing. The study results provide a reference for barrel fatigue analysis and barrel structure design. First, feature suppression by expression using a uniform parametrized template was used to realize parametric modeling of over a thousand types of barrels. Second, various models were devel-

oped for barrels with different rifling profiles during continuous firing to lay a theoretical foundation for analyzing the dynamic barrel stress during bullet engraving: a model to calculate the chamber pressure, a model to calculate heat transfer in the barrel, and a model to calculate the friction between a bullet and the wall surface of a barrel bore based on shear-slip friction theory. Then, heat-force-friction coupling during bullet engraving was comprehensively considered in constructing a finite element model, along with geometric modeling, meshing, material



model definition, setting up the load and boundary conditions, and defining contact. The dynamic barrel stress was analyzed under heat-force-friction coupling by importing two subprograms into ABAQUS: a VUAMP subprogram for calculating the chamber pressure load generated by the gunpowder combustion gas and a VFRIC subprogram for calculating the friction between the bullet and the inner barrel wall using a variable friction coefficient. The calculated chamber pressure was verified by comparison with test results. Finally, the dynamic response stress during the engraving of a bullet into four barrels with different rifling profiles during continuous firing was analyzed. The following conclusions were drawn.

- (1) For the four barrel types, a large stress is induced at the early stage of the bullet engraving into the forcing cone. As the chamber pressure keeps increasing, the bullet continues to engrave into the rifling, and the stress at the inner barrel wall continues to increase and peaks at the land/groove junctions and the entrance to the rifled section when the bullet completely engraves into the barrel. The stress subsequently trends downward. Tests revealed that all the severe damage to the various rifled barrels occurred near the entrance to the rifled section, in accordance with the simulation results
- (2) The stress distribution during projectile engraving for the barrel with rectangular rifling is substantially similar to that for the barrel with trapezoidal rifling, whereas the stress at the land/groove junctions of the barrel with rectangular rifling is generally higher than that of the barrel with trapezoidal rifling. As the groove interior angle and land exterior angle of the rectangular rifling are approximately right angles, the stress concentration at the land/groove junctions during projectile engraving is more severe for the barrel with rectangular rifling than for the barrel with trapezoidal rifling. The stress in a land is significantly higher at both sides than in the middle section, and the stress at the guide side is higher than that at the nonguide side
- (3) The stress distribution for the barrel with multiarc rifling is substantially similar to that for the barrel with multilateral-arc rifling: there is high-impact stress at the junction between the forcing cone and the rifled section, a uniform stress distribution over the rifled section, and no discernible stress concentration. Unlike the rectangular and trapezoidal rifling, the multiarc and multilateral-arc rifling feature a smooth transition between adjacent grooves and lands that facilitates bullet engraving (i.e., the engraving force is small, and there is no stress concentration). The wide lands and large area of the guide sides of the multiarc and multilateral-arc rifling help to reduce the stress at the top surface and guide side of each land. Therefore, the multiarc and multilateral-arc rifling have a considerably lower

stress at the guide side than the rectangular and trapezoidal rifling

- (4) Considering the dynamic response stress for the barrel during bullet engraving and the resulting fatigue damage, the multiarc and multilateral-arc rifling help to reduce the dynamic stress of the barrel rifling and increase the barrel fatigue life

## Data Availability

The data used to support the findings of this study are available from the corresponding author upon request.

## Conflicts of Interest

The authors declare that they have no conflicts of interest.

## References

- [1] J. Zhiming, *Gun Internal Ballistics [M]*, Beijing Institute of Technology Press, 2004.
- [2] C. Ding, N. Liu, and X. Zhang, "A mesh generation method for worn gun barrel and its application in projectile-barrel interaction analysis," *Finite Elements in Analysis and Design*, vol. 124, pp. 22–32, 2017.
- [3] C. Shen, K. Zhou, L. Ye, and J. Li, "Modeling and simulation of bullet-barrel interaction process for the damaged gun barrel," *Defence Technology*, vol. 15, no. 6, pp. 972–986, 2019.
- [4] E. Chaturvedi, "Numerical investigation of dynamic interaction with projectile and harmonic behaviour for T-finned machine gun barrels," *Defence Technology*, vol. 16, no. 2, pp. 460–469, 2020.
- [5] F. Lixia and H. Xiangyue, "Finite element simulation and analysis of projectile extrusion process [J]," *Acta Aramentarii*, vol. 32, no. 8, pp. 963–969, 2011.
- [6] B. Wu, J. Zheng, Q. Tian, Z. Zou, X. Chen, and K. Zhang, "Friction and wear between rotating band and gun barrel during engraving process," *J Wear*, vol. 318, no. 1-2, pp. 106–113, 2014.
- [7] B. Wu, J. Zheng, Q. Tian, Z. Q. Zou, X. H. Yu, and K. S. Zhang, "Tribology of rotating band and gun barrel during engraving process under quasi-static and dynamic loading[J]," *Friction*, vol. 2, no. 4, pp. 330–342, 2014.
- [8] Z. Libo, C. Yu, F. Guangbin, H. Baolin, Z. Jianlin, and L. Xianfu, "Friction model of projectile extruding into gun barrel based on temperature correction [J]," *Acta Armamentarii*, vol. 42, no. 6, pp. 1148–1156, 2021.
- [9] G. List, G. Sutter, J. J. Arnoux, and A. Molinari, "Study of friction and wear mechanisms at high sliding speed," *Mechanics of Materials*, vol. 80, pp. 246–254, 2015.
- [10] L. A. N. Weibin, *Research on the Influence of Shooting Temperature Field on the Interaction between Gun and Projectile and Shooting Accuracy [D]*, North University of China, 2018.
- [11] L. Ye, Z. Kedong, H. Lei, L. Junsong, and H. Xueying, "Research on influence of slope chamber structure parameters on internal ballistic crumpling period of guns [J]," *Acta Aramentarium*, vol. 36, no. 7, pp. 1363–1369, 2015.
- [12] G. Bixiang, Y. Zhen, and W. Chen, "Research on the influence of projectile cartridge structure parameters on the crumpling

- resistance [J],” *Fire Control & Command Control*, vol. 42, no. 3, pp. 152–155, 2017.
- [13] Z. Wei, X. Zhang, Y. Hu, and Y. Cheng, “Impact characteristics and fatigue life analysis of multi-wire recoil spring for guns,” *Shock and Vibration*, vol. 2020, 17 pages, 2020.
- [14] D. Chuanjun and Z. Xiangyan, “Simulation research on projectile belt extrusion process and internal ballistic process based on thermodynamic coupling finite element model [J],” *Acta Armamentarii*, vol. 36, no. 12, pp. 2254–2261, 2015.
- [15] C. Chuanlin, X. Huang Chenlei, L. Z. Hui, and W. Zhilin, “Experimental and numerical study on motion characteristics of small caliber rifle warhead in aftereffect period [J],” *Acta Armamentarii*, vol. 40, no. 2, pp. 265–275, 2019.
- [16] C. H. E. N. G. Yangyang, *Influence Analysis of Rifling Cross Section Shape of Different Gun Barrel on Dynamic Stress in the Process of Bullet Extrusion [D]*, North University of China, 2020.
- [17] F. Guotong, Z. Kedong, L. He, J. Wang, Z. Yingqi, and L. Junsong, “Transient heat transfer model of gun barrel under continuous fire [J],” *Journal of Ballistics*, vol. 28, no. 4, pp. 75–79, 2016.
- [18] W. A. N. G. Zhiwei, *Thermal/Structural Response Analysis of Chrome-plated Gun Barrel and Its Influence on Rim Damage [D]*, North University of China, 2019.